Reducing Rotor-Airframe Interaction Noise in sUAS Using a Curved Support Rod

Arthur D. Wiedemann * and Christopher Fuller †
Vibration and Acoustic Laboratories, Virginia Tech, Blacksburg, VA, 24061, US

Kyle A. Pascioni ‡
NASA Langley Research Center, Hampton, VA, 23681, US

Nomenclature

f = Frequency [Hz]

M_{tip} = Tip Mach number

P_B = Bandpassed power [Pa^2]

p = Acoustic pressure [Pa]

R = Rotor radius [mm]

S_{xx} = Autospectral density [Pa^2/Hz]

δ = Rotor-airframe proximity [mm]

Θ = Elevation angle [^{o}]

Φ = Azimuth angle [^{o}]

Ω = Rotation rate [rev/min]

BPF Blade Passing Frequency

CAD Computer Aided Design

OASPL Overall Sound Pressure Level

RAI Rotor-Airframe Interaction

RPM Rotations Per Minute

SALT Structural Acoustic Loads and Transmission

sUAS small Unmanned Aerial System

SPL Sound Pressure Level

*Graduate Research Assistant, Department of Mechanical Engineering, Student Member AIAA, and corresponding author warthur@vt.edu.
†Samuel Langley Distinguished Professor of Engineering, Department of Mechanical Engineering, Associate Fellow AIAA.
‡Research Aerospace Engineer, Aeroacoustics Branch.

SPSL Sound Pressure Spectrum Level

I. Introduction

Small Unmanned Aerial Systems (sUASs), commonly referred to as drones or multirotors, typically utilize several rotors distributed throughout the airframe, allowing for a lower tip speed and additional maneuverability. Rotors are typically mounted to the sUAS with a support rod. The rotor blade operates in close proximity to the rod and, as a result, creates installation noise, sometimes referred to as Rotor-Airframe Interaction (RAI) noise. Unsteady deterministic noise is generated by the aerodynamic interaction between the rotor and rod that emits an acoustic impulse event each time the blade passes the rod [1–8]. It has been observed that rapid changes in the potential flow field create impulsive changes in aerodynamic loading, which produce the impulsive acoustic noise emitted by the RAI [1, 6, 8, 9].

As the rotor approaches the rod, airflow is obstructed and slows down, creating a rapidly changing potential flow field and a rapid oscillation in the rotor angle of attack [8]. Most research studies fix the rod below the rotor because this is the typical sUAS rotor-rod configuration. It should be noted that the rod position above or below the rotor considerably affects the strength of the impulse event. When the rod is fixed above the rotor, stronger pressure fluctuations are generated on the surfaces of the rotor and rod and emit a stronger acoustic impulse [1]. When the rotor operates in close proximity to a rigid airframe, lacking any metamaterials to sheath the airframe, the pressure fluctuation on the surface of the airframe becomes the dominant noise source for the RAI [10].

The rotation rate dictates the frequency of these impulsive aerodynamic events, which results in the RAI predominantly exciting the harmonics of the blade passing frequency (BPF). While the RAI does not excite the main BPF, higher harmonics, 2×BPF to 35×BPF, can experience strong amplification, up to 30 dB, compared to an equivalent condition where the rod is not present, i.e., the isolated rotor case [2, 7]. Most excitations are concentrated at the lower harmonics, 2×BPF to 15×BPF, with the greatest excitation often around the 5×BPF for a two-bladed rotor [2].

Multiple studies have investigated the rotor performance in the presence of the rod and have either found that the average thrust slightly increased [1, 10, 11], decreased [3, 12], or had no discernible change [2, 5, 6] when the rod was present. However, rapid fluctuations were observed for the instantaneous thrust while the rotor blade approached and departed from the rod [5, 6, 11, 12]. This aerodynamic loading fluctuation creates unsteady deterministic loading noise. It produces a dipole directivity, with observers normal to the rod experiencing the strongest emission while observers colinear with the rod experience minimal excitation [1, 2, 7].

Computational [1, 2, 4–6], experimental [1, 2, 4, 7], and analytical [3, 4, 9] studies have provided insight into the interaction noise. With the physical mechanism better understood, methods of reducing the interaction noise were investigated herein. Increasing the separation distance between the rotor and the rod is the most direct method of

reducing the noise [2, 13], although, this is not always practical in reality. Adding standoffs to the rotors increased the rotor-rod proximity, resulting in an A-weighted overall sound pressure level (OASPL) reduction of 8 dBA [13]. Adding permeability to the rod weakens the surface pressure fluctuations and reduces the acoustic emission. Computational work has shown that a permeable rod could reduce the RAI noise by 20 dB at each harmonic [10]. An experimental study found that covering a solid rod with structured porous media reduced the OASPL by 3-6 dB [11].

In this study, the RAI problem is revisited experimentally. However, unlike prior studies that evaluated straight rods, the current effort focuses on RAI noise with curved rods. Curved rods should differ from straight rods as the latter generates RAI noise that is highly impulsive because the entire rotor span interacts with the rod simultaneously, thereby generating a near-simultaneous aerodynamic pressure fluctuation along the rotor blade. On the contrary, the impulsive aerodynamic phenomenon still occurs for the curved rod. However, these impulsive fluctuations do not coincide when the rod is curved. Instead, the interaction is smeared in time. Although the premise of impulsive smearing by geometric modification has been applied in other aeroacoustic problems, including swept blades for turbopropellers [14], helicopter tail rotors [15], personal air vehicles [16], and fans [17, 18], here only an augmented rod geometry was evaluated. In principle, either the rotor, rod, or both could be curved to smear the impulsive aerodynamic interaction. For this work, an experiment was conducted in hover within an anechoic chamber to measure the acoustic response for a straight and curved support rod beneath the rotor for several rotational speeds and rotor-rod separation distance to determine if the curved support rod reduces the RAI noise.

II. Experimental Setup

The investigation was conducted at NASA Langley's Structural Acoustic Loads and Transmission (SALT) facility, an anechoic chamber with wedge-tip-to-wedge-tip dimensions of 9.5, 6.5, and 4.5 m ($l \times w \times h$) rated for free-field acoustic radiation above 80 Hz [19]. Figure 1(a) shows a computer-aided design (CAD) reconstruction of the facility with 17 B&K Type 4954-B microphones stationed 2.2 m (≈10.8R) away from the rotor hub. In terms of distance from the wedge tips, the rotor is centered in the room and was fixed at a height of 2.25 m (11R) above the wedges. The CAD reconstruction shows the structure of the rotor stand and microphones, which were treated with acoustic foam for the experiment. The rotor was centered in the room and equally spaced between the floor and ceiling, resulting in the rotor being fixed 2.25 m above the wedges and oriented in the hover position. With the rotor operating in the hover configuration, the axial direction is pointed at the ceiling and defines the origin of the elevation angle, Θ. While the RAI noise more effectively excited harmonics in-plane with the rotor ($\Theta = 90^o$), it was important to consider the response for observers below the plane of rotation (e.g., $\Theta = 130^o$) because this is where a typical observer is expected to be located. Five microphones from each elevation were examined within this work to capture the directivity trends for in-plane and below to demonstrate the acoustic response to the proposed rod alteration. Microphones were evenly spaced at an azimuth of 30^o from $\Phi = 210^o$ to 330^o with the rod placed at $\Phi = 180^o$, consistent with the coordinate system of

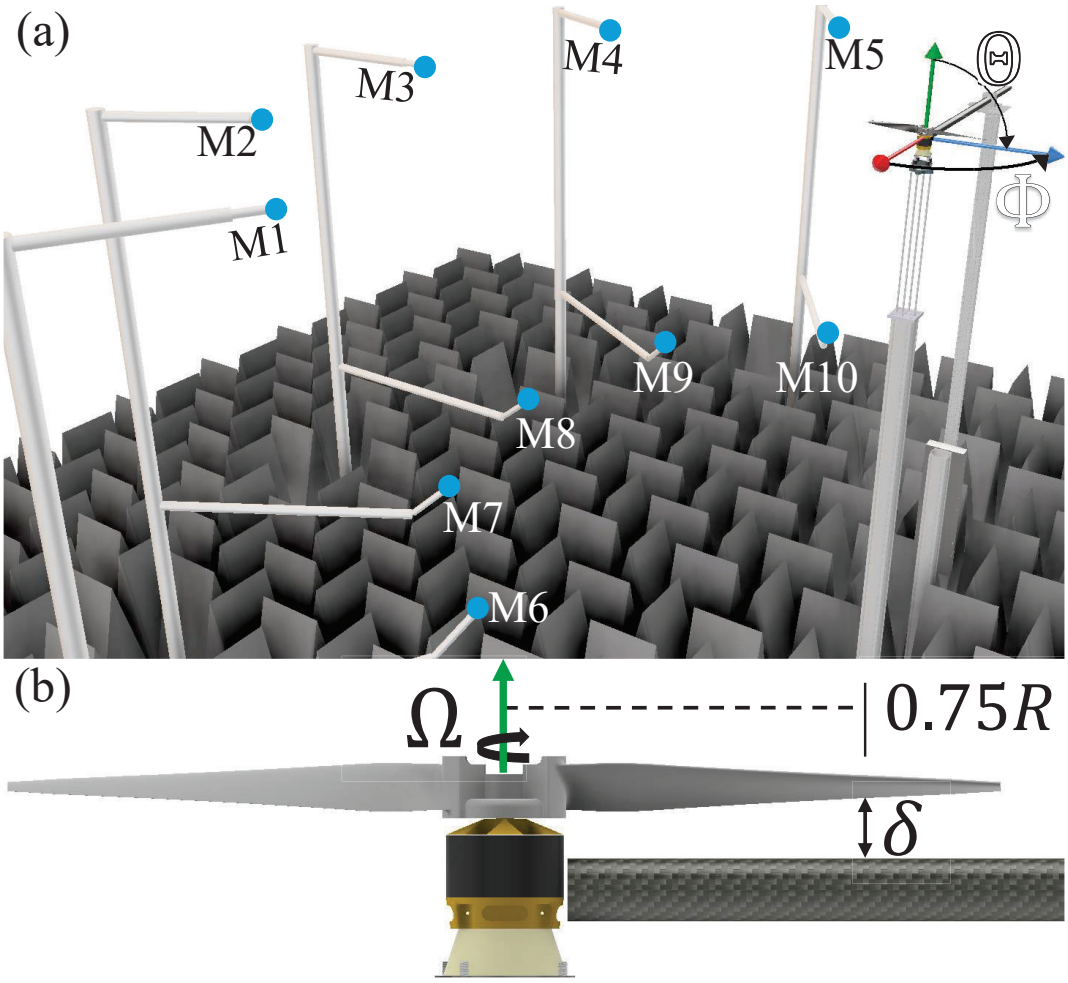

Fig. 1 CAD reconstruction of the (a) SALT facility, without the walls, with 10 microphones centered around the rotor stand and (b) a side view of the rotor.

previous work [4, 9]. Table 1 provides the Θ and Φ location for each observer. Acoustic signals were acquired on NI PXIe-4497 cards at a sample rate of 48 kHz.

Table 1 Azimuthal and elevation angle for each microphone.

Mic.	M1	M2	M3	M4	M5	M6	M7	M8	M9	M10
Θ	90°	90°	90°	90°	90°	130°	130°	130°	130°	130°
Φ	330°	300°	270°	240°	210°	330°	300°	270°	240°	210°

Figure 1(b) The rotor radius (R) is 203.2 mm and was fixed above a 25.4 mm carbon fiber rod with the proximity of δ between the rotor and rod. The rotor used was a scaled-up version of the Master Airscrew 11×8 with a 2412 NACA airfoil and was milled out of aluminum, and the chord and pitch distributions can be found in Reference [20]. The proximity between the rotor and rod was defined as the distance between the trailing edge of the rotor and the upper most point of the rod at the 75% radial location. This radial location was used because a typical rotor generates its peak

loading at this section. Figure 2(a) shows the first configuration (C1), which acts as the baseline. The new configuration (C2), shown in Fig. 2(b), replaced the straight rod with the curved rod. The curved rod was defined as the centerline of the arc length of a circle with a radius of curvature of 0.56R. This curvature was arbitrary and was meant to explore the efficacy of the curved rod in reducing RAI noise.

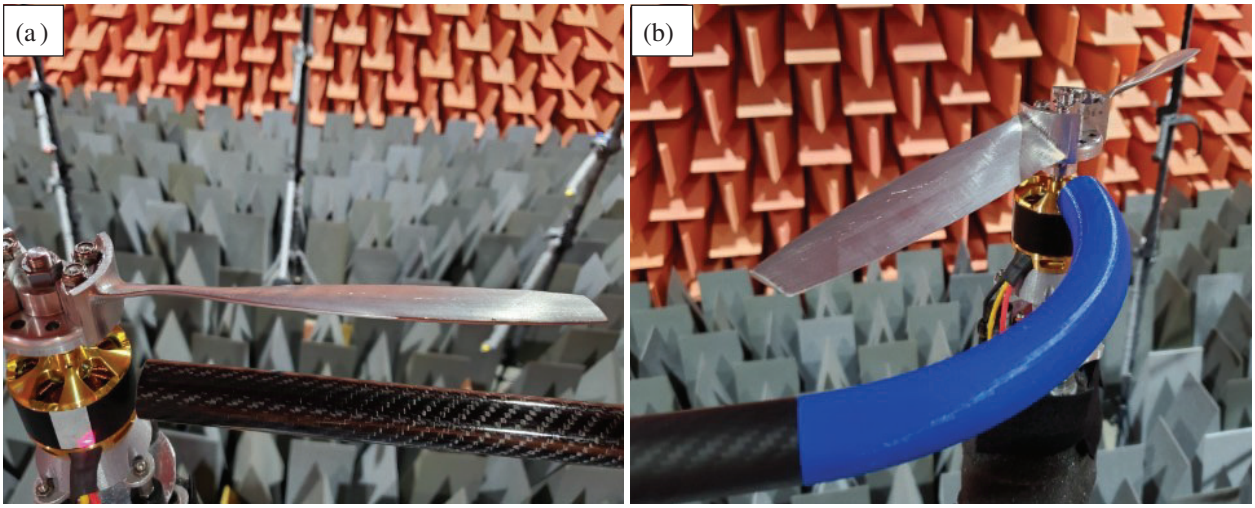

Fig. 2 The two rod configurations with (a) the straight rod, C1, and (b) curved rod, C2, underneath the rotor.

For each configuration, 16 runs were conducted at four tip Mach numbers (0.2, 0.24, 0.28, and 0.32) and four proximities (15, 20, 25, and 30 mm). These proximities are equivalent to δ/R = 0.0738, 0.0984, 0.1230, and 0.1476. Most of the analysis focused on the run conducted at 5200 RPM (M_{tip} = 0.32) and δ = 15 mm because it produced the strongest RAI response. Preliminary runs showed that runtimes above 8 seconds resulted in recirculation effects, which were important to mitigate; otherwise, turbulent airflow would have introduced unsteady loading on the rotor [21]. Comparisons between the configurations were conducted with Welch's method [22] on 8-second recordings to generate autospectral estimates using a Hanning window with 75% overlap. The block size was 4096 samples, and the 75% overlap resulted in 372 segments for each run. The resulting frequency resolution was 12 Hz.

III. Experimental Results

Literature has shown that the RAI noise emits the greatest acoustic impulse normal to the rod [2, 7]. For the straight rod, surface normals were directed at $\Phi = 270^o$, while the curved rod has surface normals pointed in all radial directions. Since the RAI noise is highly directional, caution was taken when comparing emissions at a fixed azimuth location. Directivity trends were analyzed to verify that the sound pressure level (SPL) was reduced instead of redirected. This was done with Fig. 3(a) by analyzing the SPL emission at 5×BPF for the five in-plane microphones ($\Theta = 90^o$) at the operating condition of M_{tip} = 0.32 and δ = 15 mm.

In Fig. 3(a), the directivity for the isolated, straight rod, and curved rod were compared, and the figure shows that the

straight rod had the highest SPL emission at 5×BPF. This particular harmonic was chosen because it often experienced the strongest excitation. The emission normal to C1 ($\Phi = 270^o$) was 64 dB ($p_{ref} = 20\times10^{-6}$ Pa), while C2 emitted a tone that nearly matched the isolated run, reducing the tone by 20 dB. However, C2 did not completely reduce the RAI noise, as C2 generated an acoustic emission weaker than C1 but greater than the isolated rotor, for $\Phi = 210^o$ and 240^o. These observers still experienced a significant reduction of 8 dB compared to the straight rod emission. For all microphones in the plane of rotation ($\Theta = 90^o$), C2 reduced the RAI noise substantially for this harmonic.

Fig. 3(b) shows the directivity for microphones below the plane of rotation ($\Theta = 130^o$) for the isolated, straight rod, and curved rod cases. Loading was more effectively emitted to observers below the plane of rotation than in the plane of rotation. As a result, the isolated SPL for these microphones was ≈55 dB, a 10 dB increase compared to Fig. 3(a). Depending on the observer, C1 generated an acoustic impulse 5-10 dB greater than the isolated run. Placing the curved rod in proximity to the rotor reduces the emission to 55 dB, nearly matching the isolated emission for all observers below the plane of rotation. Comparing C2 to C1, all microphones measured a reduction in SPL with the curved rod for this harmonic.

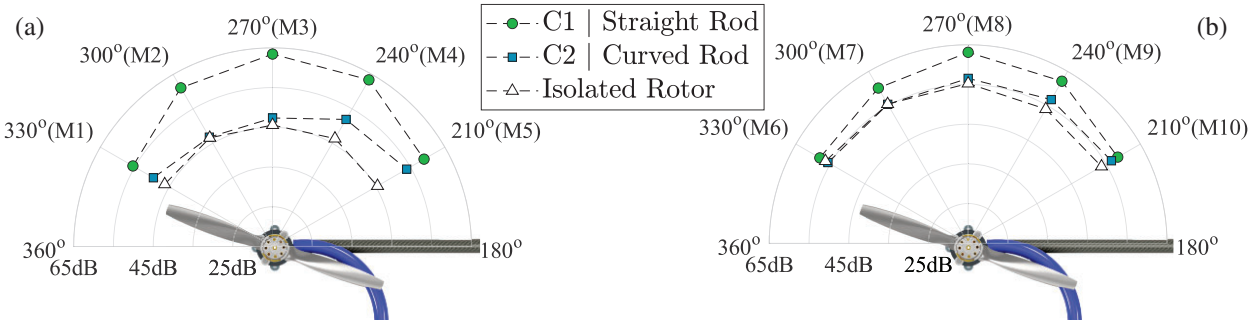

Fig. 3 SPL directivity for 5×BPF emitted (a) in-plane with the rotor ($\Theta = 90^o$) and (b) below the plane ($\Theta = 130^o$) for C1 (●), C2 (■), and the isolated rotor (△).

The acoustic emission was strongest at $\Phi = 270^o$ and $\Phi = 210^o$ for the straight and curved rods, respectively. Therefore, the sound pressure spectrum level (SPSL) was evaluated for microphones M3, M5, M8, and M10 in Fig. 4. Microphone 3 is shown in Fig. 4(a), where multiple harmonics, 2×BPF to 13×BPF, exhibited a strong tonal excitation for C1. Some harmonics were excited by as much as 20 dB because of interaction with the straight rod compared to the isolated rotor condition. Once the curved rod was installed, the emission was nearly identical to the isolated run. Emissions measured by M5 for C1, C2 and the isolated rotor are shown in Fig. 4(b). The curved rod exhibited some harmonic excitation compared to the isolated emission. However, fewer harmonics were excited to a lesser extent than C1.

The RAI emission for M8 is shown in Fig. 4(c), and the harmonic excitation above isolated rotor levels was not as significant for C1 at this elevation angle compared to the equivalent in-plane elevation angle. The curved rod reduced the

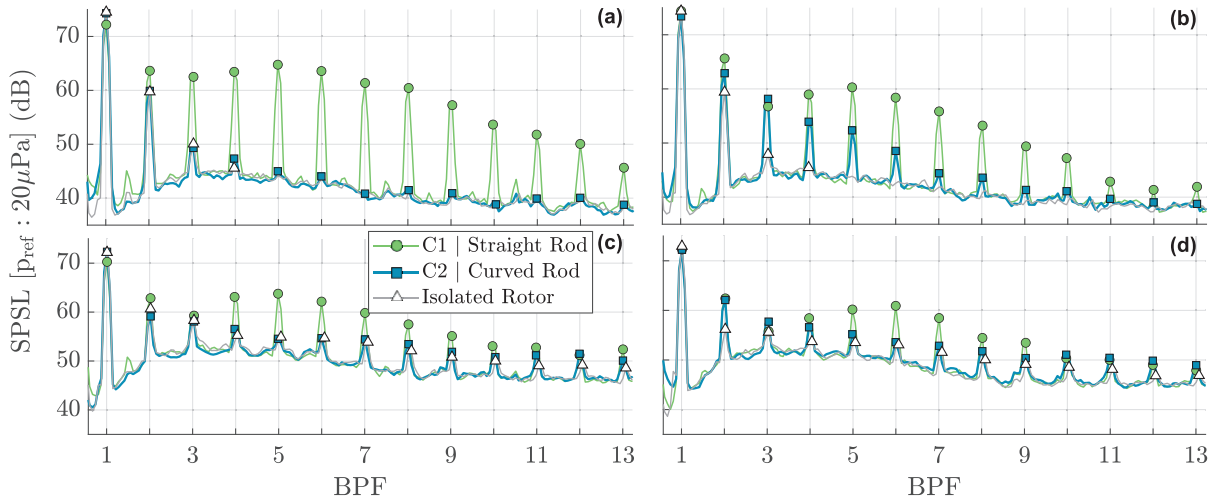

Fig. 4 Autospectra, calculated with Welch's method, for microphones (a) M3, (b) M5, (c) M8, and (d) M10 emitted by C1 (●), C2 (■), and the isolated rotor (△).

excitation by up to 8 dB for several harmonics. Lastly, Fig. 4(d) shows the emission for M10. The harmonic excitation for C2 matched C1 at 2×BPF, and was close to C1 levels at 3× and 4×BPF, but otherwise, C2 closely matched the SPSL tones of the isolated rotor. Across all observers, it was evident that C2 excited fewer harmonics to a lesser extent than C1. Across all configuration, the main BPF did not exhibit any changes in SPSL. Analytical predictions [4] suggests that the interaction weakly excites the main BPF but this excitation is dwarfed by the steady (axisymmetric) loading of the rotor.

Up to this point, only one operating condition has been analyzed. All runs from the straight and curved rods were compared to demonstrate the universal noise reduction of the curved arm. With Welch's method already estimated, autospectral density (S_{xx}) between 3×BPF and 13×BPF was integrated to estimate the bandpass power (P_B), defined as

$$P_B = \int_{3\times BPF}^{13\times BPF} S_{xx}(f)\, df, \tag{1}$$

in units of Pa^2. Equation 2 converts P_B into the bandpass sound pressure level (BSPL):

$$\mathrm{BSPL} = 10 \log_{10}\left(\frac{P_B}{\mathrm{p_{ref}}^2}\right). \tag{2}$$

The BPSL equation may seem repetitive because the SPL is estimated in the same manner. However, Eq. 1 changes the limits of integration from a region around a single harmonic to frequencies between 3×BPF and 13×BPF. Thus, it is useful to distinguish between SPL and BSPL, even if the only difference between these two metrics is the integration region. The BSPL was applied to the 16 runs for C1 and C2, and results were compared in Fig. 5 for microphone M3. All microphones showed similar trends as microphone M3, which was selected for this analysis because it measured the strongest RAI noise for C1. The BSPL emitted by C1 is shown in Fig. 5(a) as a response to $\mathrm{M_{tip}}$ and δ. Trends showed

that decreasing δ and increasing M_{tip} created a stronger tonal emission. While increasing M_{tip} strengthens the steady loading and thickness noise of the isolated rotor, the RAI noise also increased with M_{tip} because the higher rotational speed increased the potential flow field effect and pressure fluctuations on the surface of the rotor and rod. Decreasing δ increased the BSPL because a smaller interaction distance further exacerbated the potential flow field and pressure fluctuations.

The BSPL for C2 as a response to M_{tip} and δ is shown in Fig. 5(b). While the BSPL increased with M_{tip}, the BSPL was nearly independent of δ. Curving the rod reduced the RAI noise by spreading the interaction in time. Compared to C1, the curved rod also reduced the BSPL at a fixed δ and M_{tip}. Figure 5(c) shows the difference in BPSL, ΔBSPL, between C1 and C2. Implementing the curved rod reduced BSPL by 11 dB for the smallest δ. The largest δ, 30 mm, showed a more modest reduction of 4 dB. Contour lines for ΔBSPL were nearly parallel with M_{tip} because the curved rod only reduced the RAI noise and had no meaningful effect on steady loading, thickness, or broadband noise generated by the isolated rotor for the frequency range evaluated here.

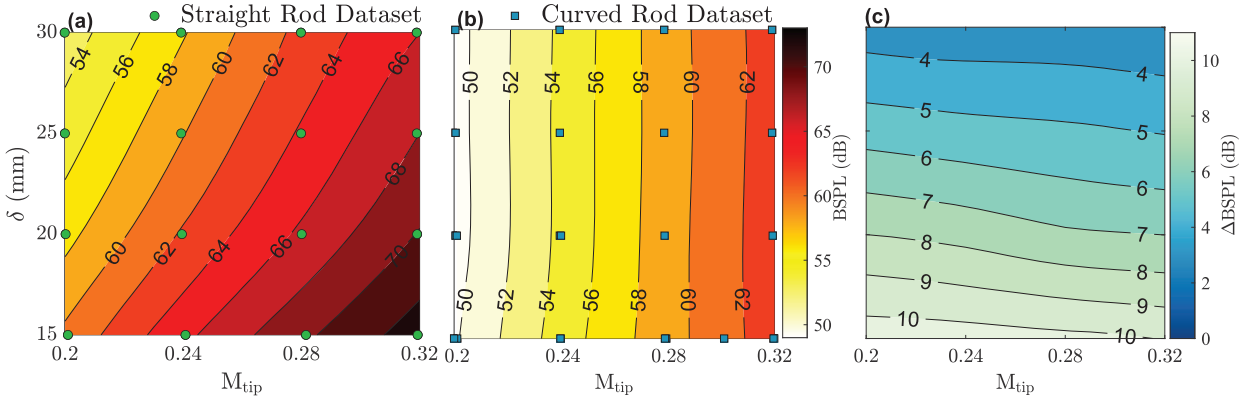

Fig. 5 BSPL for the (a) straight and (b) curved rod emission towards M3 (Φ = 270°) and (c) the difference between these configurations (C1-C2).

IV. Conclusion

This work has shown that the Rotor-Airframe Interaction noise can be significantly reduced by augmenting the shape of the rod. The curved rod diminished the RAI noise by as much as 20 dB across multiple harmonics. Microphones in-plane and below the plane of rotation experienced a reduction in sound pressure level when the curved rod was installed, often exhibiting similar levels as the isolated rotor. Directivity trends showed that the noise reduction was universal over the range of emission angles tested.

V. Acknowledgments

The authors would like to acknowledge Dr. Nikolas Zawodny, Mr. Matthew Galles, and Dr. James Stephenson of the NASA Langley Research Center for their contributions to helpful discussions, test setup, facility operations, and

data acquisition. Funding for this work was provided by the National Aeronautics and Space Administration under the NASA/NIA Cooperative Agreement NNL09AA00A.

References

[1] Zawodny, N. S., and Boyd, D. D., "Investigation of Rotor-Airframe Interaction Noise Associated with Small-Scale Rotary-Wing Unmanned Aircraft Systems," *Journal of the American Helicopter Society*, Vol. 65, No. 1, 2020, pp. 1–17. https://doi.org/doi:10.4050/JAHS.65.012007.

[2] Gojon, R., Parisot-Dupuis, H., Mellot, B., and Jardin, T., "Aeroacoustic radiation of low Reynolds number rotors in interaction with beams," *The Journal of the Acoustical Society of America*, Vol. 154, No. 2, 2023, pp. 1248–1260. https://doi.org/10.1121/10.0020672.

[3] Wu, Y., Kingan, M. J., and Go, S. T., "Propeller–strut interaction tone noise," *Physics of Fluids*, Vol. 34, No. 5, 2022. https://doi.org/10.1063/5.0090187.

[4] Vella, E., Gojon, R., Parisot-Dupuis, H., Doué, N., Jardin, T., and Roger, M., "Mutual Interaction Noise in Rotor-Beam Configuration," *30th AIAA/CEAS Aeroacoustics Conference*, 2024. https://doi.org/10.2514/6.2024-3318.

[5] Zajamšek, B., Yauwenas, Y., Doolan, C. J., Hansen, K. L., Timchenko, V., Reizes, J., and Hansen, C. H., "Experimental and numerical investigation of blade–tower interaction noise," *Journal of Sound and Vibration*, Vol. 443, 2019, pp. 362–375. https://doi.org/https://doi.org/10.1016/j.jsv.2018.11.048.

[6] Yauwenas, Y., Zajamšek, B., Reizes, J., Timchenko, V., and Doolan, C., "Directivity of blade-tower interaction noise," *JASA Express Letters*, Vol. 1, 2021. https://doi.org/10.1121/10.0005267.

[7] Wiedemann, A. D., Fuller, C., and Pascioni, K. A., "An Artificial Neural Network Approach to Predict Rotor-Airframe Acoustic Waveforms," *AIAA AVIATION 2023 Forum*, 2023. https://doi.org/10.2514/6.2023-4182.

[8] Yauwenas, Y., Zajamšek, B., Reizes, J., Timchenko, V., and Doolan, C. J., "Numerical simulation of blade-passage noise," *The Journal of the Acoustical Society of America*, Vol. 142, No. 3, 2017, pp. 1575–1586. https://doi.org/10.1121/1.5003651.

[9] Roger, M., Moreau, S., and Guédel, A., "Vortex-Shedding Noise and Potential-Interaction Noise Modeling by a Reversed Sears' Problem," *12th AIAA/CEAS Aeroacoustics Conference*, 2006. https://doi.org/10.2514/6.2006-2607.

[10] Cantos, S., Zhou, P., Ma, Z., and Li, Y., "A Numerical Study on the Reduction of Rotor Blade-Airframe Interaction Noise Through Airframe Permeability," *30th AIAA/CEAS Aeroacoustics Conference*, 2024. https://doi.org/10.2514/6.2024-3097.

[11] Crawshaw, L., Karimian, A., Paruchuri, C. C., Parry, A. B., Palleja-Cabre, S., and Arcondoulis, E., "Reduction of Propeller-Strut Interaction Noise by Porosity," *30th AIAA/CEAS Aeroacoustics Conference*, 2024. https://doi.org/10.2514/6.2024-3386.

[12] Jizhou, L., Ming, L., Kaimin, Y., and Lei, G., "Influence of fuselage arm cross-section on the aerodynamic and aeroacoustic performance of quadcopter unmanned aerial vehicles: A numerical investigation," *International Journal of Micro Air Vehicles*, Vol. 15, 2023. https://doi.org/10.1177/17568293231200281.

[13] Zawodny, N., Pettingill, N., and Thurman, C., "Identification and Reduction of Interactional Noise of a Quadcopter in Hover and Forward Flight Conditions," *INTER-NOISE and NOISE-CON Congress and Conference Proceedings*, Vol. 265, 2023, pp. 2947–2958. https://doi.org/10.3397/IN_2022_0415.

[14] Whitfield, C., Gliebe, P., Mani, R., and Mungur, P., "High speed turboprop aeroacoustic study (single rotation). Volume 1: Model Development," Tech. rep., NASA, 1989.

[15] Schneider, S., Heger, R., and Konstanzer, P., "BLUECOPTER DEMONSTRATOR: The state-of-the-art in low noise design," *42nd European Rotorcraft Forum*, 2016. https://doi.org/doi.org/10.4050/F-0073-2017-12289.

[16] Coleman, D. A., Subramanian, V., Greenwood, E., Lakshminarayan, V. K., Benedict, M., Denton, H., Halder, A., Lee, B., Runco, C., and Saemi, F., "Development of "Aria," a Compact, Quiet Personal Electric Helicopter," *Journal of the American Helicopter Society*, Vol. 68, No. 4, 2023, pp. 42011–42024. https://doi.org/doi:10.4050/JAHS.68.042011.

[17] Lucas, J., Woodward, R., and Mackinnon, M., "Acoustic evaluation of a novel swept-rotor fan," *11th Fluid and Plasma Dynamics Conference*, 1978. https://doi.org/10.2514/6.1978-1121.

[18] Zarri, A., Christophe, J., Moreau, S., and Schram, C., "Influence of Swept Blades on Low-Order Acoustic Prediction for Axial Fans," *Acoustics*, Vol. 2, No. 4, 2020, pp. 812–832. https://doi.org/10.3390/acoustics2040046.

[19] Rizzi, S. A., Cabell, R., and Allen, A. R., "Recent Enhancements to the NASA Langley Structural Acoustics Loads and Transmission (SALT) Facility," *International Conference on Recent Advances in Structural Dynamics (RASD 2013)*, 2013.

[20] Wiedemann, A., Britcher, C. P., and Fuller, C. R., "A Study of the Aeroacoustics of Swept Propellers for Small Unmanned Aerial Vehicles," *AIAA Scitech 2021 Forum*, 2021. https://doi.org/10.25777/8qwv-vq29.

[21] Stephenson, J. H., Weitsman, D., and Zawodny, N. S., "Effects of flow recirculation on unmanned aircraft system (UAS) acoustic measurements in closed anechoic chambers," *The Journal of the Acoustical Society of America*, Vol. 145, No. 3, 2019, pp. 1153–1155. https://doi.org/https://doi.org/10.1121/1.5092213.

[22] Welch, P., "The use of fast Fourier transform for the estimation of power spectra: A method based on time averaging over short, modified periodograms," *IEEE Transactions on Audio and Electroacoustics*, Vol. 15, No. 2, 1967, pp. 70–73. https://doi.org/10.1109/TAU.1967.1161901.